**PAPER** • **OPEN ACCESS**

# The Modifications of Electronic and Optical Properties of Bulk Molybdenum Disulfide by Oxygen Substitution

To cite this article: Louis Charvia *et al* 2019 *IOP Conf. Ser.: Mater. Sci. Eng.* **599** 012001



IOP Conf. Series: Materials Science and Engineering **599** (2019) 012001 doi:10.1088/1757-899X/599/1/012001

# The Modifications of Electronic and Optical Properties of Bulk Molybdenum Disulfide by Oxygen Substitution

**Louis Charvia, Shibghatullah Muhammady, Yudi Darma***

Quantum Semiconductor and Devices Lab., Department of Physics, Faculty of Mathematics and Natural Sciences, Institut Teknologi Bandung, Bandung, 40132, Indonesia

*E-mail: yudi@fi.itb.ac.id

**Abstract**. We study the electronic and optical properties of bulk $MoS_2$ and MoSO systems using the plane-wave method within the generalized gradient approximation. The structural properties show that the O substitution at S sites tunes the *z*-axis Wyckoff positions of all atoms and the bond angles. The electronic band structures show that the substitution tunes the conduction band minimum at 0.8 Σ to M and significantly promotes more localized valence states compared to that of $MoS_2$ system. The localization, mainly applying to Mo 4*d* and S 3*p* states, is more pronounced above −4 eV. Below −4 eV, O 2*p* states are dominant indicating that they are more stable than S 3*p* states. However, the substitution slightly increases the indirect and direct (K → K) bandgap of $MoS_2$ system. From the optical properties, both systems show the strong optical dichroism. By means of the substitution, the $\sigma_1$ width significantly enhances, while the plasmonic-state energy levels decrease. Our result emphasizes that the O substitution significantly tunes the electronic and optical properties of bulk $MoS_2$ system.

## 1. Introduction

Molybdenum disulfide ($MoS_2$) is a semiconducting layered transition-metal dichalcogenide (TMD) which is the most promising two-dimensional (2D) systems for nanoelectronic applications [1-4]. One of the interesting phenomena of the system is that it exhibits the layer-number-dependence of band structure. The bulk and monolayer $MoS_2$ systems have the indirect bandgap of 1.88 eV [5] and direct bandgap of 1.90 eV [1], respectively. However, the bulk system exhibits the indirect minimum bandgap ($E_g$) of 1.29 eV [5]. The reduction of the layer thickness from bulk to monolayer systems increases $E_g$, indicating the tunable band structures [6]. The monolayer system can strongly emit photons. The system exhibits the very high luminescence quantum efficiency of more than $10^4$ compared with that of the bulk system. Furthermore, the monolayer system shows the strong photoluminescence (PL) compared to the bilayer and bulk systems [1]. The defect sites in the monolayer $MoS_2$ can be used to significantly improve its hydrogen evolution activity [7]. Moreover, $MoS_2$ can also be applied in the supercapacitor by building the $MoS_2$-$H_2O$ multilayer [8] and for the energy storage by building reduced graphene oxide/$MoS_2$ hybrids [9].

The doping treatment using the transition metals at Mo site tunes the electronic and magnetic properties of $MoS_2$ system [10]. The previous experimental report has shown that the *n*-type substitution increases the local chemical affinity, while the *p*-type substitution shows the larger mobility when the electron beam exposes the system. The result emphasizes the application possibility in nanoelectronic devices [11]. The other report has shown the possibility of doping at S sites by using nonmetal and transition metal elements. The doping treatment significantly modifies the magnetic behavior of the

monolayer system. Notably, H, Br, and Cr dopings induce the half-metallic behavior of the system [12]. However, there is no report of optical properties and plasmonic states in $MoS_2$ system doped at S sites, as O and S are included in one group in the periodic table.

In this paper, we report electronic and optical properties of bulk $MoS_2$ and MoSO systems. In the MoSO system, one S atom is substituted by one O atom. We employed the plane-wave method within the generalized gradient approximation (GGA) [13]. Firstly, this paper reveals band structures and density of states from the electronic structure calculation. Secondly, the optical properties are calculated in the term of energy-dependent optical conductivity ($\sigma_1$), which is extracted from the imaginary part of dielectric function ($\varepsilon_2$). Lastly, the electron-energy loss function (L) also calculated to indicates the plasmonic-state energy levels.

## 2. Computational details

Quantum ESPRESSO package code [14, 15] was carried out for calculating the electronic and optical properties of unit cells of bulk $MoS_2$ and MoSO systems. The crystal structure models of both systems visualized by VESTA [16] are presented in figure 1. The structural parameters in this calculation are directly adopted from the previous experimental report. At room temperature, the bulk $MoS_2$ exhibits the hexagonal crystal structure with the structural parameters of $a$ = 3.15 Å, $c$ = 12.30 Å, $z_S$ = 0.621 within the space group of $P6_3/mmc$ [17]. Each Mo atom is surrounded by O atoms within the triangular prismatic shape. From top view along $c$-axis, the hexagonal pattern consists of 3 Mo and 3 S atoms [18]. For MoSO system, two O atom substitute one S atom at atomic positions of (2/3, 1/3, $-z$) and (1/3, 2/3, $-z + 1/2$) in the unit cell of MoSO system. We employed the Perdew-Burke-Ernzerhof (PBE)-type exchange-correlation functional energy for all atoms within the GGA method [13]. This method was used for various systems in our previous reports [19-21]. All-electron potentials are approached by the norm-conserving pseudopotentials [22-24]. The calculation carried out kinetic cutoff energy of 1.6 keV, a Γ-point-centered $k$-point mesh of 7 × 7 × 2, and threshold energy of 10 meV. All atomic positions are optimized using the 'relax' calculation with threshold force of 50 meV/Å involving the Broyden–Fletcher–Goldfarb–Shanno (BFGS) algorithm [25-28]. On the other hand, the lattice parameters ($a$ and $c$) are set to be constant.

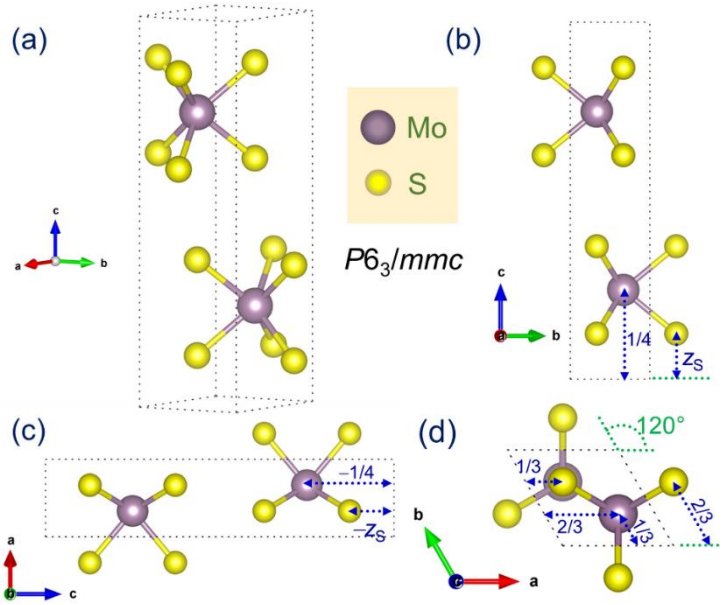


**Figure 1.** Crystal structure of bulk $MoS_2$ for views along (a) diagonal, (b) $a$, (c) $b$, and (d) $c$ axes. The Wyckoff positions of Mo and S atoms are Mo (2$c$: 1/3, 2/3, 1/4) and S (4$f$: 1/3, 2/3, $z_S$).

The Drude-Lorentz model [29] is used in the optical properties calculation. This model covers the interband and intraband parts of complex dielectric functions ($\varepsilon$) [30]. From both parts, $\varepsilon$ is divided into real and imaginary parts of dielectric functions ($\varepsilon_1$, $\varepsilon_2$) which are connected by the K ramers-Kronig relation [31, 32]. Both $\varepsilon_1$, $\varepsilon_2$ will be reported elsewhere in future. In this paper, we show the imaginary-part optical conductivity ($\sigma_1$) expressed as

$$\sigma_1 = \frac{\omega \varepsilon_2}{4\pi} \tag{1}$$

where $\omega$ is the photon frequency. We also reveal the loss function ($L$) spectrum calculated by

$$L = -\mathrm{Im}\left\{\frac{1}{\varepsilon}\right\} = \frac{\varepsilon_2}{\varepsilon_1^2 + \varepsilon_2^2} \tag{2}$$

The energy-dependent $L$ can accurately assign plasmonic-state energy levels [32].

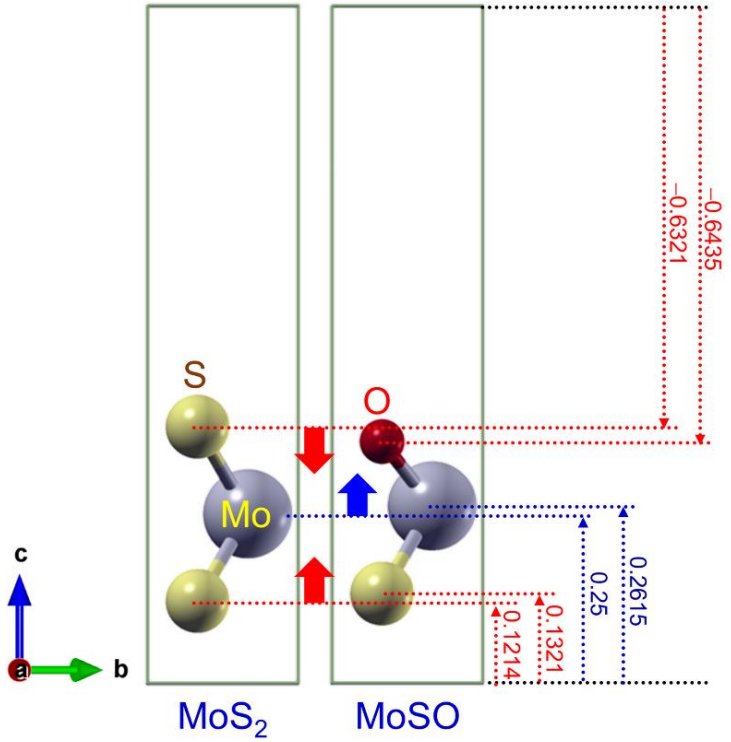


**Figure 2**. Schematic illustration of shifts of $z$-axis atomic positions in $MoS_2$ system induced by the O substitution at S site in MoSO system.

**Table 1**. Optimized Wyckoff positions of $MoS_2$ and MoSO systems.

| Atom | Atomic positions ($x$, $y$, $z$) ($a$ = $b$ = 3.15 Å and $c$ = 12.30 Å) | | |
|---|---|---|---|
| | $MoS_2$ | | MoSO |
| | Present work | Previous experiment [17] | |
| Mo (2*c*) | 1/3, 2/3, 1/4 | 1/3, 2/3, 1/4 | 1/3, 2/3, 0.2615 |
| S (4*f*) | 1/3, 2/3, $z_S$ ($z_S$ = 0.6214) | 1/3, 2/3, $z_S$ ($z_S$ = 0.621) | 1/3, 2/3, $z_S$ ($z_S$ = 0.6321) |
| O (4*f*) | – | – | 1/3, 2/3, $z_O$ ($z_O$ = 0.6435) |

## 3. Results and Discussions

### *3.1. Structural properties*

Firstly, we investigate the structural optimization results of both $MoS_2$ and MoSO systems. Table 1 presents optimized Wyckoff positions of both systems. As the results, the present calculation well reproduces the experimental results [17]. On the other hand, the O substitution at S sites slightly modifies the atomic positions. The *z*-axis Wyckoff position of all atoms increases. The result indicates the atomic bonding modifications. Figure 2 presents the schematic illustration of shifts of the *z*-axis atomic positions, which is visualized by XCrysDEN [33]. We find that the S–Mo–S bond angle of 82.012° decreases to 73.921° as the O–Mo–S bond angle. The previous report shows the S–Mo–S bond angle of 82.207° [17]. Hence, the structural properties of $MoS_2$ system in the present work is comparable with the previously reported results. We suggest that the structural properties of MoSO system can also be used to predict experimental results.

### *3.2. Electronic properties*

Figure 3 presents the band structures of bulk $MoS_2$ and MoSO systems. We find the indirect $E_g$ = 0.94 eV from Γ to 0.8Σ points in $MoS_2$ system, which is lower than that of the previous experimental report, i.e., 1.29 eV from reflectivity [5] and *L* spectra [34]. The underestimated $E_g$ can be caused by the limitation of GGA in describing the exact Kohn-Sham band structure within GGA [35]. We also find the direct transition at K point of 2.66 eV. The band structures show the delocalized states along Γ–M and K–Γ points, indicated by the delocalized valence-band feature. However, the localized states are found along M–K points, which are indicated by the localized valence-band feature.

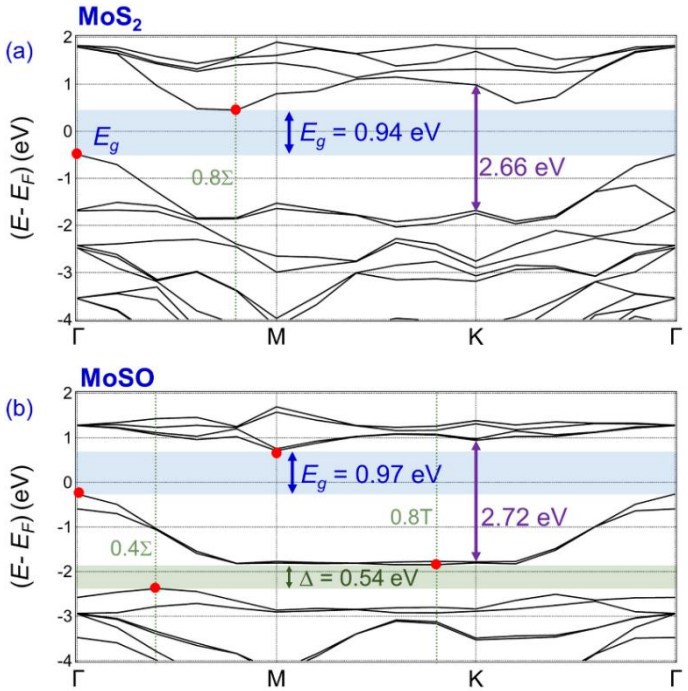


**Figure 3**. Band structures of bulk (a) $MoS_2$ and (b) MoSO systems. Indirect and direct bandgaps are assigned. The blue shades denote the minimum bandgap ($E_g$) of both systems, while the green shade denotes the bandgap (Δ) within the valence band of MoSO system. The red dots denote the points involved in the indirect band transitions. Fermi energy level ($E_F$) is denoted at 0 eV.

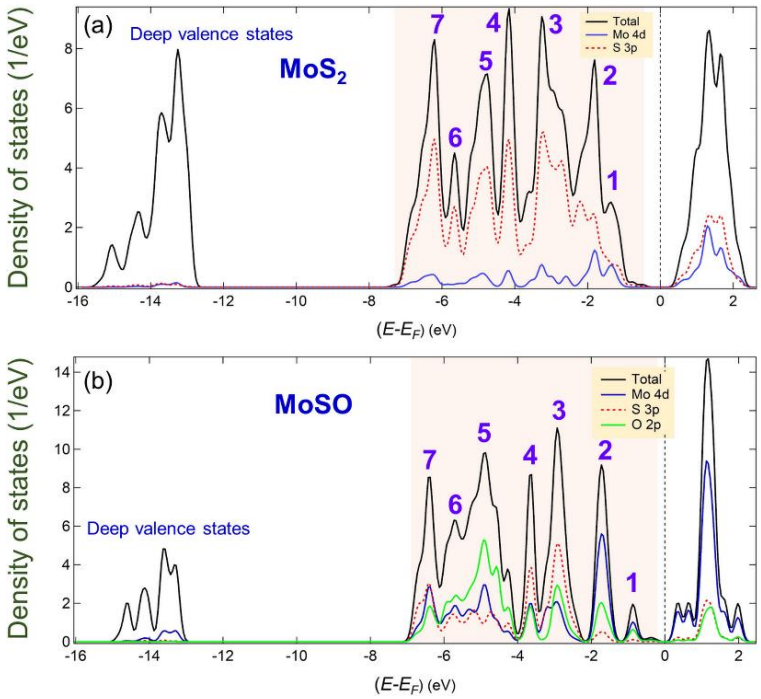


**Figure 4**. Total and partial density of states of bulk (a) $MoS_2$ and (b) MoSO systems. Near Fermi energy level ($E_F$), the width and peaks of valence band are assigned by the soft red shade and numbers (1 to 7), respectively. Fermi energy level ($E_F$) is denoted at 0 eV.

MoSO system shows the indirect $E_g$ of 0.97 eV from Γ to M points. This result shows that the substitution slightly increases $E_g$. However, it changes the transition point at the conduction band minimum from 0.8Σ path to M point. This result is different with that of the monolayer $MoS_2$, as revealed by the previous first-principle calculation. The O substitution at S site in the monolayer $MoS_2$ does not only change the transition point but also changes $E_g$ type from direct to indirect types [36]. We also find the in-valence-band interband transition (Δ) of 0.54 eV from 0.4Σ to 0.8T paths. The presence of Δ is induced by the localized valence band feature at around −2 eV. The band structure also indicates the localized states for all *k*-points. Hence, the substitution significantly promotes more localized valence states.

Figure 4(a) shows the total and partial density of states (DOS) of bulk $MoS_2$ system. We find that $MoS_2$ system shows $E_g$ around Fermi energy level ($E_F$), which mainly promoted by Mo 4*d*, followed by S 3*p* states. Near $E_F$, the valence band is dominated by S 3*p*. This result approves the theoretical electron configuration of $S^{2-}$: [37] $3s^2\ 3p^6$. However, the conduction band is dominated by both Mo 4*d* and S 3*p* states. The presence of Mo 4*d* states in the conduction band approves the partially occupied $Mo^{2+}\ 4d^2$ orbital. The presence of S 3*p* states may be resulted due to the strong hybridization between Mo 4*d* and S 3*p* states. We also assign seven peaks (1-7) in the valence band. All seven peaks overlap each other, indicating the dominant delocalized states, as presented in figure 3(a).

Figure 4(b) presents the total and partial density of states (DOS) of bulk MoSO system. We find that $E_g$ is mainly promoted by Mo 4*d* and O 2*p* states. The conduction band is dominated by Mo 4*d* states approving the valence electron configuration of $Mo^{2+}\ 4d^2$. Interestingly, more complex features in the valence band are observable. Seven peaks in the valence band of MoSO system are assigned. We find that the peaks 1-4 are localized above −4 eV, which are in contrast to that of $MoS_2$ system. This result confirms the localized bands in figure 3(b). However, the peaks 5-7 below −4 eV are delocalized, as also found in $MoS_2$ system in figure 4(a). Hence, the substitution significantly modifies the valence band structure alignment of $MoS_2$ system near $E_F$.

### *3.3. Optical properties*

Figure 5 presents the energy-dependence of $\sigma_1$ bulk $MoS_2$ and MoSO systems. In $MoS_2$ system, we find different curves of $\sigma_1$ along *xy* plane ($\sigma_{1xy}$) and *z* axis ($\sigma_{1z}$), as shown in figure 5(a). This result indicates optical dichroism, which has also been found in $\alpha$-PbO [38] and $TiO_2$-based systems [39]. The optical dichroism indicates that the bulk $MoS_2$ is anisotropic, as previously shown by different dielectric constants along different directions (*xy*-plane and *z*-axis) [40]. In region A, two major peaks are observed for both *xy*-plane and *z*-axis directions. The peak shape is similar, indicating the weak dichroism in this region. In region B, we find high peak at around 5.7 eV along *z* axis, while *xy* plane does not show any significant peak. This result indicates the strong dichroism in the region. Between both regions A and B, a major peak at around 4.5 eV is found for *xy* plane. Figure 5(b) also shows the optical dichroism in MoSO system. In contrast to $MoS_2$ system, both regions A and B show strong optical dichroism along both *xy*-plane and *z*-axis directions, indicated by the significant different shapes between $\sigma_1$ of both systems. Notably, region A of MoSO system shows the multiple peaks at which their intensities are lower than that of the double peaks of $MoS_2$ system. We suggest that the presence of multi-peaks are induced by the transitions between the localized valence states near $E_F$ to conduction states. Furthermore, $\sigma_1$ width (~7.16 eV) of MoSO system is wider than that of $MoS_2$ system (~6.39 eV), indicating the wider absorption range in MoSO system.

Figure 6 presents *L* of bulk $MoS_2$ and MoSO systems. In the *L* spectrum, the peaks represent plasma energy as the oscillatory response of delocalized valence electrons due to the plasma excitation. This excitation is induced by the inelastic scattering between the atomic electrons in a material and an electron beam. The excitation results when the speed of electron beam is higher than the Fermi velocity [41]. Figure 6(a) shows two *L* peaks at 11.3 and 12.1 eV along *xy*-plane ($L_{xy}$) in $MoS_2$ system. At the lower energy level of 10.9 eV along *z* axis, we find a higher peak compared to both other peaks. All these peaks imply the plasmonic states. This result indicates the dichroism of plasmonic state. By considering the difference between energy levels for the peaks at 11.3 and 10.9 eV, the dichroism is 0.4 eV. Figure 6(b) shows two *L* peaks at 10.9 and 11.3 eV along *xy*-plane ($L_{xy}$) in MoSO system. A peak at 9.5 eV is also found along *z* axis ($L_z$). By considering the difference between energy levels for the peaks at 10.9 and 9.5 eV, the dichroism of MoSO system is 1.4 eV, which indicates that MoSO system exhibit the higher plasmonic-state dichroism than that of $MoS_2$ system. Additionally, plasmonic-state width is also increased by the substitution (green shade).

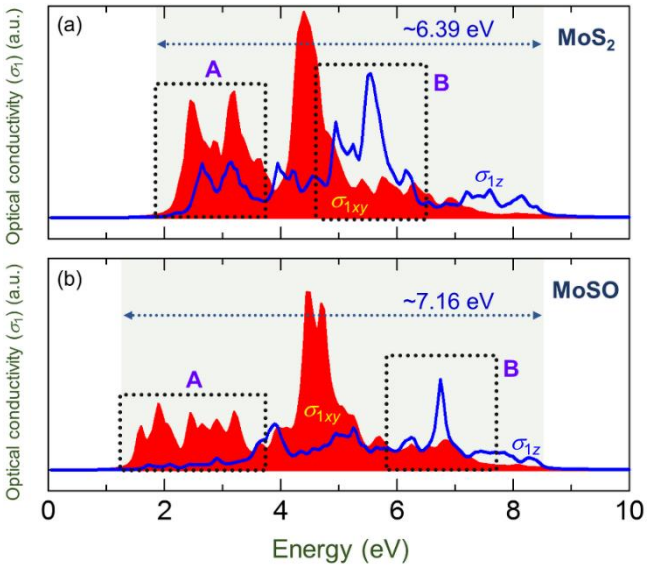


**Figure 5**. Optical conductivity ($\sigma_1$) of bulk (a) $MoS_2$ and (b) MoSO systems. Red face and blue line denote $\sigma_1$ along *xy* plane ($\sigma_{1xy}$) and *z* axis ($\sigma_{1z}$), respectively. The $\sigma_1$ width is assigned by the green shade. The dashed squares (A and B) emphasize the significant $\sigma_1$ modification.

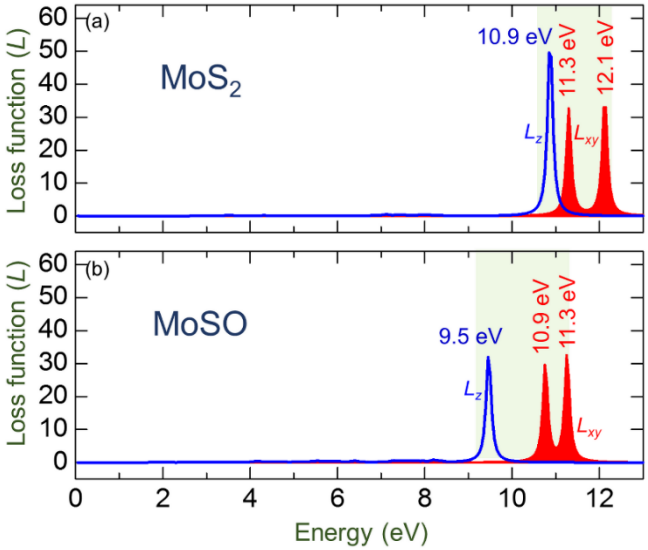


**Figure 6**. Electron-energy loss function ($L$) of bulk (a) $MoS_2$ and (b) MoSO systems. Red face and blue line denote $L$ along $xy$ plane ($L_{xy}$) and $z$ axis ($L_z$), respectively. The green shade denotes the plasmonic-state width.

## 4. Conclusions

We have studied the electronic and optical properties of bulk $MoS_2$ and MoSO systems using the GGA. As the results, the structural properties show that the O substitution modifies the $z$-axis Wyckoff positions of atoms as well as the bond angles between cations (Mo) and anions (O or S). The substitution also tunes the conduction band minimum and provokes more localized valence states compared to that of $MoS_2$ system. We find that the localization is more pronounced above –4 eV, which mainly comes from Mo 4$d$ and S 3$p$ states. On the other hand, O 2$p$ states are dominant below –4 eV. However, there is only a small shift of $E_g$ due to the substitution. Furthermore, the optical properties show that both systems show the strong optical dichroism of $\sigma_1$ and $L$. The substitution significantly increases the $\sigma_1$ width and decreases the plasmonic-state energy levels. This study shows the significant tuning of the electronic and optical properties of bulk $MoS_2$ system by the O substitution at S sites.

## 5. References

[1] Mak K F, Lee C, Hone J, Shan J and Heinz T F 2010 *Phys. Rev. Lett.* **105** 136805
[2] Radisavljevic B, Radenovic A, Brivio J, Giacometti V and Kis A 2011 *Nat. Nanotechnol.* **6** 147
[3] Lee H S, Min S-W, Chang Y-G, Park M K, Nam T, Kim H, Kim J H, Ryu S and Im S 2012 *Nano Lett.* **12** 3695
[4] Radisavljevic B and Kis A 2013 *Nature Mater.* **12** 815
[5] Beal A R and Hughes H P 1979 *J. Phys. C: Solid State Phys.* **12** 881
[6] Kumar A and Ahluwalia P K 2012 *Eur. Phys. J. B* **85** 186
[7] Ye G, Gong Y, Lin J, Li B, He Y, Pantelides S T, Zhou W, Vajtai R and Ajayan P M 2016 *Nano Lett.* **16** 1097
[8] Geng X, Zhang Y, Han Y, Li J, Yang L, Benamara M, Chen L and Zhu H 2017 *Nano Lett.* **17** 1825
[9] Cheng T, Xu J, Tan Z, Ye J, Tao Z, Du Z, Wu Y, Wu S, Ji H and Yu Y 2018 *Energy Storage Mater.* **10** 282
[10] Cheng Y C, Zhu Z Y, Mi W B, Guo Z B and Schwingenschlögl U 2013 *Phys. Rev. B* **87** 100401
[11] Lin Y C, Dumcenco D O, Komsa H P, Niimi Y, Krasheninnikov A V, Huang Y S and Suenaga K 2014 *Adv. Mater.* **26** 2857
[12] Yue Q, Chang S, Qin S and Li J 2013 *Phys. Lett. A* **377** 1362

[13] Perdew J P, Burke K and Ernzerhof M 1996 *Phys. Rev. Lett.* **77** 3865
[14] Giannozzi P, Baroni S, Bonini N, Calandra M, Car R, Cavazzoni C, Ceresoli D, Chiarotti G L, Cococcioni M, Dabo I, Corso A D, Gironcoli S d, Fabris S, Fratesi G, Gebauer R, Gerstmann U, Gougoussis C, Kokalj A, Lazzeri M, Martin-Samos L, Marzari N, Mauri F, Mazzarello R, Paolini S, Pasquarello A, Paulatto L, Sbraccia C, Scandolo S, Sclauzero G, Seitsonen A P, Smogunov A, Umari P and Wentzcovitch R M 2009 *J. Phys.: Condens. Matter* **21** 395502
[15] Giannozzi P, Andreussi O, Brumme T, Bunau O, Nardelli M B, Calandra M, Car R, Cavazzoni C, Ceresoli D and Cococcioni M 2017 *J. Phys.: Condens. Matter* **29** 465901
[16] Momma K and Izumi F 2011 *J. Appl. Crystallogr.* **44** 1272
[17] Dickinson R G and Pauling L 1923 *J. Am. Chem. Soc.* **45** 1466
[18] Kadantsev E S and Hawrylak P 2012 *Solid State Commun.* **152** 909
[19] Muhammady S, Kurniawan Y, Ishiwata S, Rousuli A, Nagasaki T, Nakamura S, Sato H, Higashiya A, Yamasaki A, Hara Y, Rusydi A, Takase K and Darma Y 2018 *Inorg. Chem.* **57** 10214
[20] Muhammady S, Sutjahja I M, Rusydi A, Winata T, Takase K and Darma Y 2017 *Jpn. J. Appl. Phys.* **56** 121201
[21] Muhammady S, Kurniawan Y, Rusydi A and Darma Y 2019 *J. Phys. Chem. Solids* **125** 16
[22] Troullier N and Martins J L 1990 *Solid State Commun.* **74** 613
[23] Troullier N and Martins J L 1991 *Phys. Rev. B* **43** 1993
[24] Troullier N and Martins J L 1991 *Phys. Rev. B* **43** 8861
[25] Broyden C G 1970 *IMA J. Appl. Math.* **6** 76
[26] Fletcher R 1970 *Comput. J.* **13** 317
[27] Goldfarb D 1970 *Math. Comput.* **24** 23
[28] Shanno D F 1970 *Math. Comput.* **24** 647
[29] Fujiwara H 2007 *Spectroscopic ellipsometry: principles and applications* (West Sussex: John Wiley & Sons Ltd)
[30] Rakić A D, Djurišić A B, Elazar J M and Majewski M L 1998 *Appl. Optics* **37** 5271
[31] Sturm K 1982 *Adv. Phys.* **31** 1
[32] Dressel M and Guner G 2005 *Electrodynamics of solids: Optical Properties of Electrons in Matter* (Cambridge: Cambridge University Press)
[33] Kokalj A 1999 *J. Mol. Graphics Modell.* **17** 176
[34] Hong J, Li K, Jin C, Zhang X, Zhang Z and Yuan J 2016 *Phys. Rev. B* **93** 075440
[35] Perdew J P 1985 *Int. J. Quantum Chem.* **28** 497
[36] Kong L-J, Liu G-H and Qiang L 2016 *Comput. Mater. Sci.* **111** 416
[37] Mak K F and Shan J 2016 *Nature Photonics* **10** 216
[38] Kurniawan Y, Muhammady S, Widita R and Darma Y 2019 *Mater. Res. Express* **6** 055908
[39] Muhammady S, Nurfani E, Kurniawan R, Sutjahja I M, Winata T and Darma Y 2017 *Mater. Res. Express* **4** 024002
[40] Saigal N, Sugunakar V and Ghosh S 2016 *Appl. Phys. Lett.* **108** 132105
[41] Egerton R F 2008 *Rep. Prog. Phys.* **72** 016502

**Acknowledgments**
Our work was funded by Ministry of Research, Technology, and Higher Education of Indonesia through Hibah Kompetensi Kemenristekdikti 2018, Penelitian Dasar Unggulan Perguruan Tinggi (PDUPT) program 2018 (532w/l1.C01/PL/2018), P3MI and Riset ITB 2019 research program.